Stability of the fcc structure in block copolymer systems

2008 J. Phys.: Condens. Matter 20 465104

(http://iopscience.iop.org/0953-8984/20/46/465104)

J. Phys.: Condens. Matter **20** (2008) 465104 (9pp) doi:10.1088/0953-8984/20/46/465104

Stability of the fcc structure in block copolymer systems

Makiko Nonomura

Department of Mathematical and Life Sciences, Graduate School of Sciences, Hiroshima University, 1-3-1 Higashi-Hiroshima, 739-8526, Japan

E-mail: nonomura@hiroshima-u.ac.jp

Received 12 June 2008, in final form 3 September 2008
Published 21 October 2008
Online at stacks.iop.org/JPhysCM/20/465104

Abstract

The stability of the face-centered cubic (fcc) structure in microphase separated copolymers is investigated by a coarse-grained approach. Direct simulations of the equation for the microphase separation in three dimensions indicate that there is a narrow area above a certain degree of segregation in the phase diagram, where the fcc structure is the most stable structure. By employing the mode expansion, we have confirmed that the fcc structure can form as a metastable structure even in the weak segregation regime.

1. Introduction

The face-centered cubic (fcc) phase has been observed in various sphere-formed systems, as has the body-centered cubic (bcc) structure. Colloids, surfactants, and atomic systems are representative examples. Recently, the fcc structure has been observed in block copolymer solutions [1, 2], in diblock/homopolymer blend [3], and in triblock copolymer systems [4]. On the other hand, in the limit of pure diblock copolymer melts there have been no experiments that have shown that the fcc structure is stable.

The morphological transitions of A–B type diblock copolymer melts have been investigated using the mode expansion method [5–10]. The time evolution of the microphase separated structures was investigated by solving the amplitude equations of various fundamental modes. The four equilibrium structures (lamellar, bcc, hexagonal cylinder, and gyroid) observed in the weak segregation regime have been studied by taking into account the modes with the gyroid symmetry [8]. The $Fddd$ structure has been reported in [11] as another equilibrium phase. The recent theories of block copolymers are summarized in [12].

In [9], amplitude equations were derived for the fcc symmetry with the sufficient numbers of modes expressing the fcc structure, but the fcc solution was found to be unstable. On the other hand, Matsen and Bates reported the existence of a narrow region in the phase diagram in which the close-packed spheres (of either fcc structure or hexagonal close-packed structure) are stable [13, 14]. This discrepancy was attributed to the fact that either the mode expansion in such segregation regimes is invalid or that the free energy is too simple to contain the fcc structure. However, even if these assumptions are correct, the reason why only the fcc structure cannot be investigated by the mode expansion method remains unclear.

The purpose of the present paper is to investigate the fcc structure in thermal equilibrium by more accurate mode expansion and by numerical simulations. The free energy functional employed in previous studies is also used herein [15]:

$$F[\phi] = \int \mathrm{d}\boldsymbol{r}\left[\tfrac{1}{2}(\nabla\phi)^2 + W(\phi)\right] + \frac{\alpha}{2}\int \mathrm{d}\boldsymbol{r}\int \mathrm{d}\boldsymbol{r}' G(\boldsymbol{r},\boldsymbol{r}')\left(\phi(\boldsymbol{r})-\bar{\phi}\right)\left(\phi(\boldsymbol{r}')-\bar{\phi}\right), \quad (1)$$

where

$$W(\phi) = -\frac{\tau}{2}\phi^2 + \frac{g}{4}\phi^4. \quad (2)$$

The variable ϕ represents the local volume fraction difference between A and B monomers, i.e. $\phi = \phi_\mathrm{A} - \phi_\mathrm{B}$, where ϕ_A (ϕ_B) is the local volume fraction of the A (B) monomers. The incompressibility condition $\phi_\mathrm{A} + \phi_\mathrm{B} = 1$ has been imposed. The coefficients α and g are positive constants and $\bar{\phi}$ is the spatial average of ϕ. The parameter τ is negative at the high-temperature uniform phase and positive for the microphase separated state at low temperature. The function $G(\boldsymbol{r},\boldsymbol{r}')$ in the second term of equation (1) is defined through the following relation:

$$-\nabla^2 G = \delta(\boldsymbol{r}-\boldsymbol{r}'). \quad (3)$$

The time evolution equation for ϕ is given by [16]

$$\frac{\partial\phi}{\partial t} = \nabla^2\frac{\delta F}{\delta\phi} = \nabla^2(-\nabla^2\phi - \tau\phi + g\phi^3) - \alpha(\phi-\bar{\phi}). \quad (4)$$

The parameters in equation (1) are connected to the parameters in self-consistent field theory (SCFT) [13, 14]. Noting that equation (1) is rescaled by the coefficient $D_\phi = \ell^2/(12a(1-a))$ in front of $(\nabla\phi)^2/2$, it is found that $\tau = \chi/D_\phi$, $\alpha = 9/(D_\phi N^2 \ell^2 a^2(1-a)^2)$ and $g \propto 1/D_\phi$, where the Flory–Huggins interaction parameter χ, the index of polymerization measuring the number of monomers per macromolecule N, the block ratio of A-block a and the Kuhn statistical length ℓ [17].

In the present study, the phase diagram is given by direct simulation of equation (4) including the fcc structure as well as other equilibrium structures. Furthermore, the mode expansion method is employed by taking account of the higher harmonics of the fundamental modes of the fcc symmetry. The obtained results by the mode expansion are applicable to other sphere-forming systems in the weak segregation limit, even though the free energy of the diblock copolymers is considered initially.

The organization of the present paper is as follows. In section 2, the equilibrium phase diagram obtained by the direct simulations is presented. In section 3, a coupled set of equations for amplitudes is derived by the mode expansion, and a linear stability analysis is performed. A summary and discussion are presented in section 4. The form of the free energy and the amplitude equations for the bcc structure are given in the appendix.

2. Numerical simulation

The direct simulations of the time evolution given by equation (4) are carried out by employing the semi-implicit scheme [18]. The value of $\phi^{(n+1)}$ at the $n+1$ step is computed by using the value of $\phi^{(n)}$ of the previous step as $[1/\mathrm{d}t + \nabla_\mathrm{d}^4 - g\nabla_\mathrm{d}^2 D(\phi^{(n)})^2 + \alpha]\phi^{(n+1)} = (1/\mathrm{d}t - \tau\nabla_\mathrm{d}^2)\phi^{(n)} + \alpha\bar{\phi}$, where the discrete Laplacian ∇_d and a diagonal matrix $D(\phi^{(n)})$ whose diagonal components are given by $\phi^{(n)}$. The time increment $\mathrm{d}t$ is set to 0.1. The simulation box is divided into $32 \times 32 \times 32$ grids. The initial values of ϕ are provided by the small cosine modulations of the target structures. The periodic boundary conditions are imposed. The coefficients of g and α are fixed as $g = \alpha = 1$ throughout the simulations. In order to make the periodicity adjust to its equilibrium, the linear length of the simulation box L is regarded as a dynamical variable. Its time evolution is assumed to be given by the following fictitious equation of motion [19]:

$$\frac{\mathrm{d}L}{\mathrm{d}t} = -\mu\frac{\partial(F/V)}{\partial L}, \tag{5}$$

where F is the total free energy and V is the total volume of the system. This equation gives us the period for the minimum value of the free energy. The increment of the length is set to 0.0001 and $\mu = 100$. The space mesh size is given by $L/32$.

Figure 1 shows the angular-averaged power spectrum $I(q)$ of the equilibrium structures obtained by the direct simulations. We obtain the characteristic peak positions following the ratios of $1{:}\sqrt{4/3}{:}\sqrt{8/3}{:}\sqrt{11/3}{:}\sqrt{12/3}\cdots$ for fcc lattice and the ratios of $1{:}\sqrt{2}{:}\sqrt{3}{:}\sqrt{4}\cdots$ for bcc lattice [20]. The forms of $I(q)$ of the fcc structure for $\tau = 2.10$ and $\bar{\phi} = 0.15$ and for $\tau = 2.70$ and $\bar{\phi} = 0.60$ are shown in figures 1(a) and (c), respectively. Figures 1(b) and (d) are the $I(q)$ of the bcc for $\tau = 2.10$ and $\bar{\phi} = 0.15$ and the $I(q)$ of the bcc for $\tau = 2.70$ and $\bar{\phi} = 0.60$, respectively. It is noted that the $\sqrt{4/3}$ peak of the fcc structure for $\tau = 2.10$ and $\bar{\phi} = 0.15$ is comparable to that of the first peak in figure 1(a), whereas the $\sqrt{2}$ bcc peak is 100 times less than the first peak in figure 1(b).

The spatial averaged free energy of the structures $F_\mathrm{ave} = F/V$ can be evaluated by substituting the obtained data of $\phi(\boldsymbol{r})$ at $t \to \infty$ into equation (1). The values of F_ave for the fcc structure and for the bcc structure are obtained as $F_\mathrm{ave} = -2.388\,20 \times 10^{-2}$ and $F_\mathrm{ave} = -2.407\,43 \times 10^{-2}$ for $\tau = 2.10$ and $\bar{\phi} = 0.15$, and $F_\mathrm{ave} = -0.454\,545$ and $F_\mathrm{ave} = -0.454\,519$ for $\tau = 2.70$ and $\bar{\phi} = 0.60$, respectively. This means that the fcc structure has a higher energy than the bcc structure for $\tau = 2.10$ and $\bar{\phi} = 0.15$, whereas the fcc structure becomes more stable than the bcc structure for $\tau = 2.70$ and $\bar{\phi} = 0.60$. Therefore, one may conclude that the fcc structure exists as a stable equilibrium structure above a certain degree of segregation.

In the same way, the spatial averaged free energies of lamellar, hexagonal cylinder, gyroid, and $Fddd$ are evaluated. Comparing these free energies, the phase diagram in the τ–$\bar{\phi}$ plane is obtained in figure 2. A small area was found in which the free energy of the fcc structure is the lowest. This phase diagram is qualitatively consistent with that obtained by Matsen and Bates by the SCFT [13, 14], with the exception that the phase diagram of the present study contains the region in which the $Fddd$ structure is most stable, as reported in [10, 11].

In this section, it is found by employing the simple free energy (1) that there is the narrow region where the fcc structure becomes the most stable. The fcc solutions can be stable even in the weak segregation regime, whereas it has been reported in [9] that the fcc solution was unstable by the one-mode expansion. In order to clarify the reason for this discrepancy, the linear stability analysis by more accurate mode expansion will be carried out in section 3.

3. Mode expansion

The weak segregation limit is considered and the variable ϕ is expanded as follows:

$$\phi(\boldsymbol{r}) = \bar{\phi} + 2\sum_{i=1}^{7} f_i \cos(\boldsymbol{q}_i \cdot \boldsymbol{r}), \tag{6}$$

where f_i are real amplitudes. The seven reciprocal lattice vectors are given by

$$\begin{aligned} \boldsymbol{q}_1 &= \frac{Q}{\sqrt{3}}(1,1,1), & \boldsymbol{q}_2 &= \frac{Q}{\sqrt{3}}(1,-1,1), \\ \boldsymbol{q}_3 &= \frac{Q}{\sqrt{3}}(-1,1,1), & \boldsymbol{q}_4 &= \frac{Q}{\sqrt{3}}(1,1,-1), \\ \boldsymbol{q}_5 &= \frac{Q}{\sqrt{3}}(2,0,0), & \boldsymbol{q}_6 &= \frac{Q}{\sqrt{3}}(0,2,0), \\ & & \boldsymbol{q}_7 &= \frac{Q}{\sqrt{3}}(0,0,2). \end{aligned} \tag{7}$$

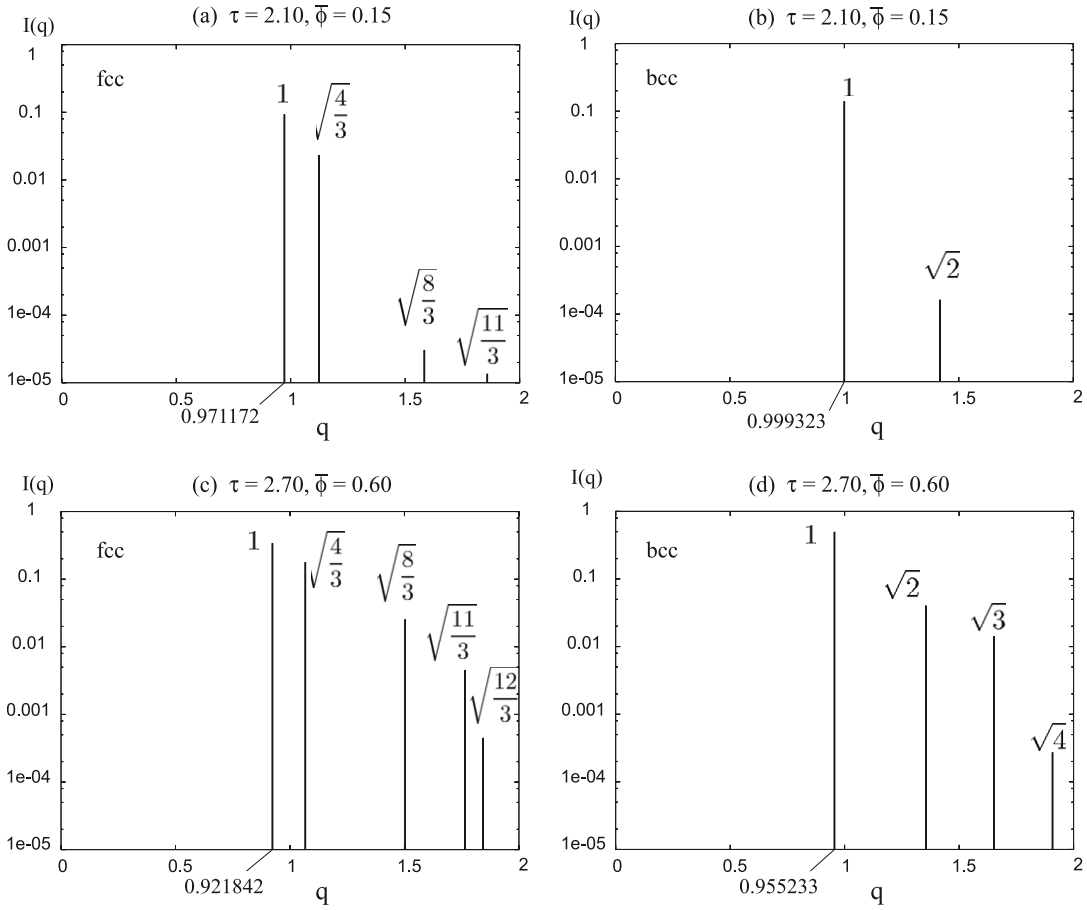

Figure 1. Angular-averaged power spectra $I(q)$ presented as a function of wavenumber $q = |\boldsymbol{q}|$.

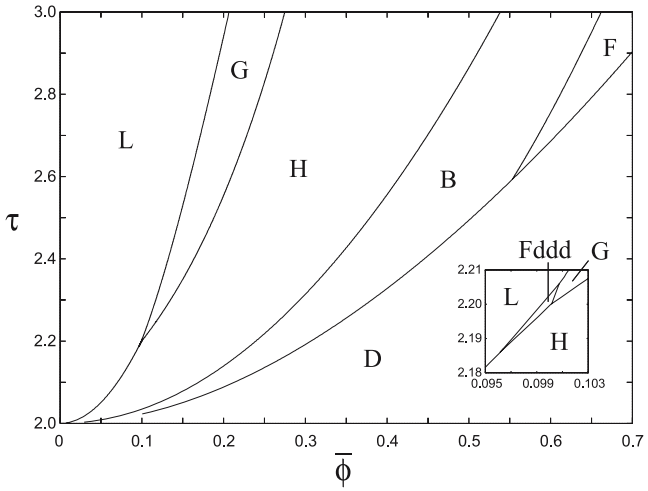

Figure 2. Phase diagram obtained by the direct simulation of equation (4). The regions indicated by L, G, H, B, F, and D are the stable phase of lamellae, gyroid, hexagons, bcc, fcc, and disorder, respectively. The insert is the enlargement near the triple point G, L, and H, where the $Fddd$ structure is the most stable structure.

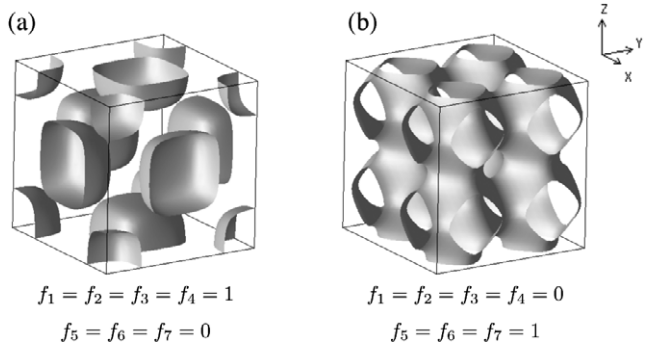

Figure 3. The structures expressed by the reciprocal vectors of the fcc structure (a) and the next highest harmonics (b) in the isosurface representation with $\phi_{\mathrm{ISO}} = 1.0$.

The first four vectors of equation (7) produce the fcc structure, as shown in figure 3(a). The other vectors, $\boldsymbol{q}_5$, $\boldsymbol{q}_6$, and $\boldsymbol{q}_7$ have not been considered in the previous paper [9]. If only f_5, f_6, and f_7 are non-zero and are of the same magnitude, then equation (6) represents the Schwarz P surface as shown in figure 3(b). From equation (7), it is obvious that $|\boldsymbol{q}_i| = Q$ $(i = 1, 2, 3, 4)$ and $|\boldsymbol{q}_j| = 2Q/\sqrt{3}$ $(j = 5, 6, 7)$. The higher modes in equation (6) compose the peaks for which the position is $\sqrt{4/3}$ times that of the first peak in figures 1(a) and (c). It is noted that more accurate expansions are needed by taking into account the higher modes if the mode expansion method is applied above a certain degree of segregation such as $\tau = 2.70$ and $\bar{\phi} = 0.60$ as shown in figure 1(c).

Substituting equation (6) into equation (4), a coupled set of amplitude equations is obtained as follows:

$$\frac{\mathrm{d}f_1}{\mathrm{d}t} = -|\boldsymbol{q}_1|^2 g\Big[\Gamma(|\boldsymbol{q}_1|)f_1 - 3f_1^3 + 6f_1\sum_{i=1}^{7} f_i^2 + 6\bar{\phi}f_2f_6 + 6\bar{\phi}f_3f_5 + 6\bar{\phi}f_4f_7 + 6f_2f_3f_4 + 6f_2f_5f_7 + 6f_3f_6f_7 + 6f_4f_5f_6\Big] \quad (8)$$

$$\frac{\mathrm{d}f_2}{\mathrm{d}t} = -|\boldsymbol{q}_2|^2 g\Big[\Gamma(|\boldsymbol{q}_2|)f_2 - 3f_2^3 + 6f_2\sum_{i=1}^{7} f_i^2 + 6\bar{\phi}f_1f_6 + 6\bar{\phi}f_3f_7 + 6\bar{\phi}f_4f_5 + 6f_1f_3f_4 + 6f_1f_5f_7 + 6f_3f_5f_6 + 6f_4f_6f_7\Big] \quad (9)$$

$$\frac{\mathrm{d}f_3}{\mathrm{d}t} = -|\boldsymbol{q}_3|^2 g\Big[\Gamma(|\boldsymbol{q}_3|)f_3 - 3f_3^3 + 6f_3\sum_{i=1}^{7} f_i^2 + 6\bar{\phi}f_1f_5 + 6\bar{\phi}f_2f_7 + 6\bar{\phi}f_4f_6 + 6f_1f_2f_4 + 6f_1f_6f_7 + 6f_2f_5f_6 + 6f_4f_5f_7\Big] \quad (10)$$

$$\frac{\mathrm{d}f_4}{\mathrm{d}t} = -|\boldsymbol{q}_4|^2 g\Big[\Gamma(|\boldsymbol{q}_4|)f_4 - 3f_4^3 + 6f_4\sum_{i=1}^{7} f_i^2 + 6\bar{\phi}f_1f_7 + 6\bar{\phi}f_2f_5 + 6\bar{\phi}f_3f_6 + 6f_1f_2f_3 + 6f_1f_5f_6 + 6f_2f_6f_7 + 6f_3f_5f_7\Big] \quad (11)$$

$$\frac{\mathrm{d}f_5}{\mathrm{d}t} = -|\boldsymbol{q}_5|^2 g\Big[\Gamma(|\boldsymbol{q}_5|)f_5 - 3f_5^3 + 6f_5\sum_{i=1}^{7} f_i^2 + 6\bar{\phi}f_1f_3 + 6\bar{\phi}f_2f_4 + 6f_1f_2f_7 + 6f_1f_4f_6 + 6f_2f_3f_6 + 6f_3f_4f_7\Big] \quad (12)$$

$$\frac{\mathrm{d}f_6}{\mathrm{d}t} = -|\boldsymbol{q}_6|^2 g\Big[\Gamma(|\boldsymbol{q}_6|)f_6 - 3f_6^3 + 6f_6\sum_{i=1}^{7} f_i^2 + 6\bar{\phi}f_1f_2 + 6\bar{\phi}f_3f_4 + 6f_1f_3f_7 + 6f_1f_4f_5 + 6f_2f_3f_5 + 6f_2f_4f_7\Big] \quad (13)$$

$$\frac{\mathrm{d}f_7}{\mathrm{d}t} = -|\boldsymbol{q}_7|^2 g\Big[\Gamma(|\boldsymbol{q}_7|)f_7 - 3f_7^3 + 6f_7\sum_{i=1}^{7} f_i^2 + 6\bar{\phi}f_1f_4 + 6\bar{\phi}f_2f_3 + 6f_1f_2f_5 + 6f_1f_3f_6 + 6f_2f_4f_6 + 6f_3f_4f_5\Big]. \quad (14)$$

The coefficient of the linear term of each amplitude equation is given as a function of the wavenumber by

$$\Gamma(x) = \frac{1}{g}\left(x^2 + \frac{\alpha}{x^2} - \tau + 3\bar{\phi}^2 g\right). \quad (15)$$

Similarly, the free energy given by equation (1) can also be written in terms of the amplitudes f_i as

$$F_{\mathrm{fcc}} = F_{\mathrm{dis}} + g\Big[\sum_{i=1}^{7}\Gamma(|\boldsymbol{q}_i|)f_i^2 + \frac{3}{2}\sum_{i=1}^{7} f_i^4 + 6\sum_{i=1}^{7}\sum_{j=i+1}^{7} f_i^2 f_j^2 + 12f_1f_2f_3f_4 + 12(f_1f_3 + f_2f_4)(\bar{\phi}f_5 + f_6f_7) + 12(f_1f_2 + f_3f_4)(\bar{\phi}f_6 + f_5f_7) + 12(f_1f_4 + f_2f_3)(\bar{\phi}f_7 + f_5f_6)\Big], \quad (16)$$

where $F_{\mathrm{dis}} = -\frac{\tau}{2}\bar{\phi}^2 + \frac{g}{4}\bar{\phi}^4$ is the free energy for the disorder state. The equilibrium period Q_* of the periodic structures should be determined by the minimization of the free energy (16), $\frac{\partial F_{\mathrm{fcc}}}{\partial Q}|_{Q=Q_*} = 0$, as

$$Q_*^4 = \alpha\left(12\sum_{i=1}^{4} f_i^2 + 9\sum_{i=5}^{7} f_i^2\right)\Big/\left(12\sum_{i=1}^{4} f_i^2 + 16\sum_{i=5}^{7} f_i^2\right). \quad (17)$$

Setting $f_5 = f_6 = f_7 = 0$, the set of amplitude equations, equations (8)–(11), agree with the set in the previous paper [9]. In [9], two types of equilibrium solutions were reported. The first is $f_1 = f_2$ and $f_3 = f_4$, and the second is $f_1 = f_2 = f_3$ and f_4. By drawing their nullclines, the fcc structure $f_1 = f_2 = f_3 = f_4 \neq 0$ has been concluded to be unstable.

However, solving the entire set of the amplitude equations, equations (8)–(14), numerically, the solution $f_1 = f_2 = f_3 = f_4 \neq 0$ was found to become stable with $f_5 = f_6 = f_7 \neq 0$. For instance, $f_1 = f_2 = f_3 = f_4 = -5.376\,92 \times 10^{-2}$ and $f_5 = f_6 = f_7 = -2.985\,50 \times 10^{-2}$ are obtained numerically for $\alpha = g = 1$, $\tau = 2.10$ and $\bar{\phi} = 0.15$. In fact, substituting $f_1 = f_2 = f_3 = f_4 = A$ and $f_5 = f_6 = f_7 = B$ into equations (8) and (12), we obtain the following reduced equations:

$$\frac{\mathrm{d}A}{\mathrm{d}t} = -Q^2 g\left(\Gamma(Q)A + 27A^3 + 36AB^2 + 18AB\bar{\phi}\right) \quad (18)$$

$$\frac{\mathrm{d}B}{\mathrm{d}t} = -\frac{4}{3}Q^2 g\left(\Gamma\left(\frac{2Q}{\sqrt{3}}\right)B + 48A^2B + 15B^3 + 12A^2\bar{\phi}\right). \quad (19)$$

It is obvious that there are no solutions $A \neq 0$ and $B = 0$ because of the $A^2\bar{\phi}$ term in equation (19). In other words, since the homogenized amplitude equations require that both $A \neq 0$ and $B \neq 0$, the effect of taking into account the higher modes is not a simple perturbation but leads to qualitatively as well as quantitatively different results from those of the single mode approximation. Therefore, the higher harmonic modes must be considered for the fcc structure as written in [21]. In the remainder of this section, a linear stability analysis is performed around $f_1 = f_2 = f_3 = f_4 = f$.

From equation (17), the equilibrium period is obtained as

$$Q_*^4 = \alpha \frac{48 + 9(\eta_5^2 + \eta_6^2 + \eta_7^2)}{48 + 16(\eta_5^2 + \eta_6^2 + \eta_7^2)}, \tag{20}$$

where $\eta_j = f_j/f$, $(j = 5, 6, 7)$. Substituting equation (20) into equation (15), the function $\Gamma(Q_*)$ is written as a function of η_5, η_6 and η_7, called $\Gamma_*(\eta_5, \eta_6, \eta_7)$. On the other hand, substituting $f_1 = f_2 = f_3 = f_4 = f$ and $\mathrm{d}f/\mathrm{d}t = 0$ into equation (8), we obtain

$$\Gamma_*(\eta_5, \eta_6, \eta_7) = -3f^2(9 + 2\eta_5^2 + 2\eta_6^2 + 2\eta_7^2 + 2\eta_5\eta_6 + 2\eta_6\eta_7 + 2\eta_7\eta_5) - 6f\bar{\phi}(\eta_5 + \eta_6 + \eta_7). \tag{21}$$

Therefore, the condition $\Gamma_*(\eta_5, \eta_6, \eta_7) < 3(\eta_5 + \eta_6 + \eta_7)^2\bar{\phi}^2/(9 + 2\eta_5^2 + 2\eta_6^2 + 2\eta_7^2 + 2\eta_5\eta_6 + 2\eta_6\eta_7 + 2\eta_7\eta_5)$ must be satisfied in order for the real solution of f to exist.

The stability of the fcc solution can be examined by substituting $f_i = f + a_i (i = 1, 2, 3, 4)$ into equations (8)–(11) and retaining only the linear terms of the deviations a_i:

$$\frac{\mathrm{d}}{\mathrm{d}t}\begin{pmatrix} a_1 \\ a_2 \\ a_3 \\ a_4 \end{pmatrix} = T \begin{pmatrix} a_1 \\ a_2 \\ a_3 \\ a_4 \end{pmatrix} \quad \text{with}$$

$$T = 6f \begin{pmatrix} T_{\mathrm{dia}} & T_6 & T_5 & T_7 \\ T_6 & T_{\mathrm{dia}} & T_7 & T_5 \\ T_5 & T_7 & T_{\mathrm{dia}} & T_6 \\ T_7 & T_5 & T_6 & T_{\mathrm{dia}} \end{pmatrix}, \tag{22}$$

where $T_{\mathrm{dia}} = (\eta_5 + \eta_6 + \eta_7)\bar{\phi} + (\eta_5\eta_6 + \eta_6\eta_7 + \eta_7\eta_5)f$, $T_5 = -(3 + \eta_6\eta_7)f - \eta_5\bar{\phi}$, $T_6 = -(3 + \eta_7\eta_5)f - \eta_6\bar{\phi}$ and $T_7 = -(3 + \eta_5\eta_6)f - \eta_7\bar{\phi}$. Diagonalizing equation (22), the equations $\partial_t u_i = \lambda_i u_i$, $(i = 1, \ldots 4)$ are obtained, where

$$\lambda_1 = -54f^2 \tag{23a}$$

$$\lambda_2 = 6f^2(3 + 2\eta_7\eta_5 + 2\eta_6\eta_7) + 12f(\eta_5 + \eta_6)\bar{\phi} \tag{23b}$$

$$\lambda_3 = 6f^2(3 + 2\eta_5\eta_6 + 2\eta_6\eta_7) + 12f(\eta_7 + \eta_5)\bar{\phi} \tag{23c}$$

$$\lambda_4 = 6f^2(3 + 2\eta_5\eta_6 + 2\eta_7\eta_5) + 12f(\eta_6 + \eta_7)\bar{\phi}, \tag{23d}$$

and

$$u_1 = \frac{a_1 + a_2 + a_3 + a_4}{4} \tag{24a}$$

$$u_2 = \frac{a_1 - a_2 - a_3 + a_4}{4} \tag{24b}$$

$$u_3 = \frac{-a_1 - a_2 + a_3 + a_4}{4} \tag{24c}$$

$$u_4 = \frac{-a_1 + a_2 - a_3 + a_4}{4}. \tag{24d}$$

The sign of the eigenvalues is examined as follows. The eigenvalue λ_1 is always negative, and the signs of the other eigenvalues become positive $\lambda_2 = \lambda_3 = \lambda_4 = 18f^2 > 0$ in the case of $\eta_5 = \eta_6 = \eta_7 = 0$. By solving the system of equations $u_1 \neq 0$ and $u_2 = u_3 = u_4 = 0$, the solution with fcc symmetry $a_1 = a_2 = a_3 = a_4 = u_1$ is obtained. The gray region in figure 4 indicates that the eigenvalue $\lambda_2 = 6f^2(3+2(\zeta - m)\kappa)$ becomes negative, where $m = -\bar{\phi}/f$, $\zeta = \eta_7$ and $\kappa = \eta_5 + \eta_6$. The case $u_2 = \ell_0 \neq 0$ and $u_1 = u_3 = u_4 = 0$ provides the solution $a_1 = -a_2 = -a_3 = a_4 = \ell_0$, which grows in the white region in figure 4. Note that m is positive because of the relation $f\bar{\phi} < 0$ in [7]. The same figure can be used for λ_3 with $\zeta = \eta_6$ and $\kappa = \eta_7 + \eta_5$ and for λ_4 with $\zeta = \eta_5$ and $\kappa = \eta_6 + \eta_7$.

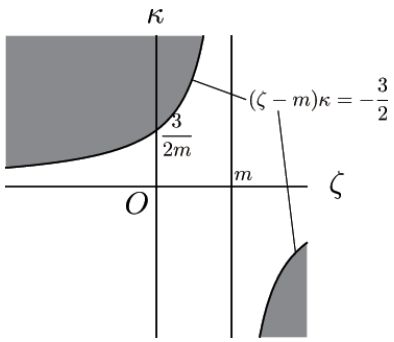

Figure 4. Contour plot of $\lambda_2 = 6f^2(3 + 2(\zeta - m)\kappa)$ on the ζ–κ plane, where $m = -\bar{\phi}/f$, $\zeta = \eta_7$ and $\kappa = \eta_5 + \eta_6$. The gray color indicates the region of $\lambda_2 < 0$, in which the fcc structure is linearly stable.

There are two other combinations of u_i. One is the case that $u_1 = 0$ and $u_2 = u_3 = u_4 \equiv \ell_1$, that is $a_1 = a_2 = a_3 = -\ell_1$ and $a_4 = 3\ell_1$. The other is the case that $u_1 = 0$, $u_2 = \ell_2$ and $u_3 = u_4 = \ell_3$, i.e., $a_1 = \ell_2 - 2\ell_3$, $a_2 = a_3 = -\ell_2$, and $a_4 = \ell_2 + 2\ell_3$. Assembling these deviations, the amplitudes f_i $(i = 1, \ldots, 4)$ are written as

$$f_1 = f - \ell_1 + \ell_2' - 2\ell_3 \tag{25a}$$

$$f_2 = f - \ell_1 - \ell_2' \tag{25b}$$

$$f_3 = f - \ell_1 - \ell_2' \tag{25c}$$

$$f_4 = f + 3\ell_1 + \ell_2' + 2\ell_3, \tag{25d}$$

where $\ell_2' = \ell_0 + \ell_2$. Figures 5(a)–(c) display the structures of the deviations obtained by substituting equations (25*a*)–(25*d*) with (a) $\ell_1 = 1$ and $f = \ell_2' = \ell_3 = 0$, (b) $\ell_2' = 1$ and $f = \ell_1 = \ell_3 = 0$, and (c) $\ell_3 = 1$ and $f = \ell_1 = \ell_2' = 0$, into equation (6), respectively. Similarly, the structures in figure 6 are obtained by changing the values of ℓ_1 and ℓ_2' in equations (25*a*)–(25*d*) while keeping f fixed ($f = 1$).

Comparing with the statement given in the paragraph just below equation (17), we note that the deviations ℓ_1 and ℓ_2' correspond to the two types of equilibrium solutions of the one-mode expansion [9]. If the magnitudes of the deviation are equivalent to that of the fcc structure, the structures become lamellar (figure 6(a) $\ell_1 = 1$), diamond (figure 6(a) $\ell_1 = -1$), and distorted cylinder (figure 6(b) $\ell_2' = \pm 1$) structures, which have been reported as stable solutions in the case of the one-mode expansion [9].

The amplitude equations and the free energy for the bcc structure obtained by including higher order harmonics, are given in appendix. The stability of the bcc solution is not influenced by the higher modes. For example, the amplitudes are obtained as $b_i = -5.349\,96 \times 10^{-2}$ $(i = 1, \ldots, 6)$ by solving equations (A.4)–(A.9) with $b_j = 0$ $(j = 7, 8, 9)$ for $\alpha = g = 1$, $\tau = 2.10$ and $\bar{\phi} = 0.15$. On the other hand, the entire set of amplitude equations, equations (A.4)–(A.12),

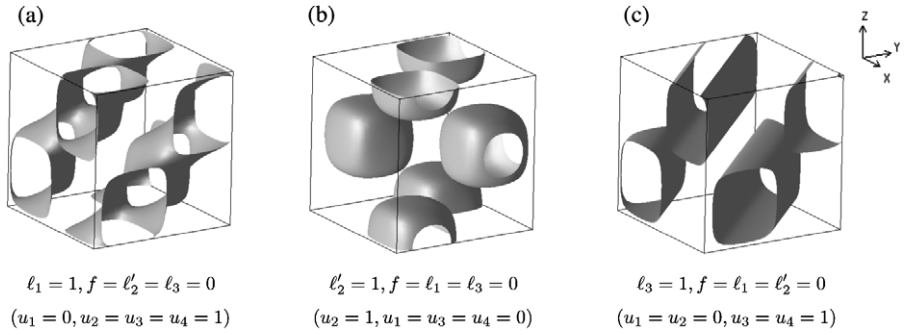

Figure 5. Structure of the deviations in the isosurface representation with $\phi_{\mathrm{ISO}} = 1.0$.

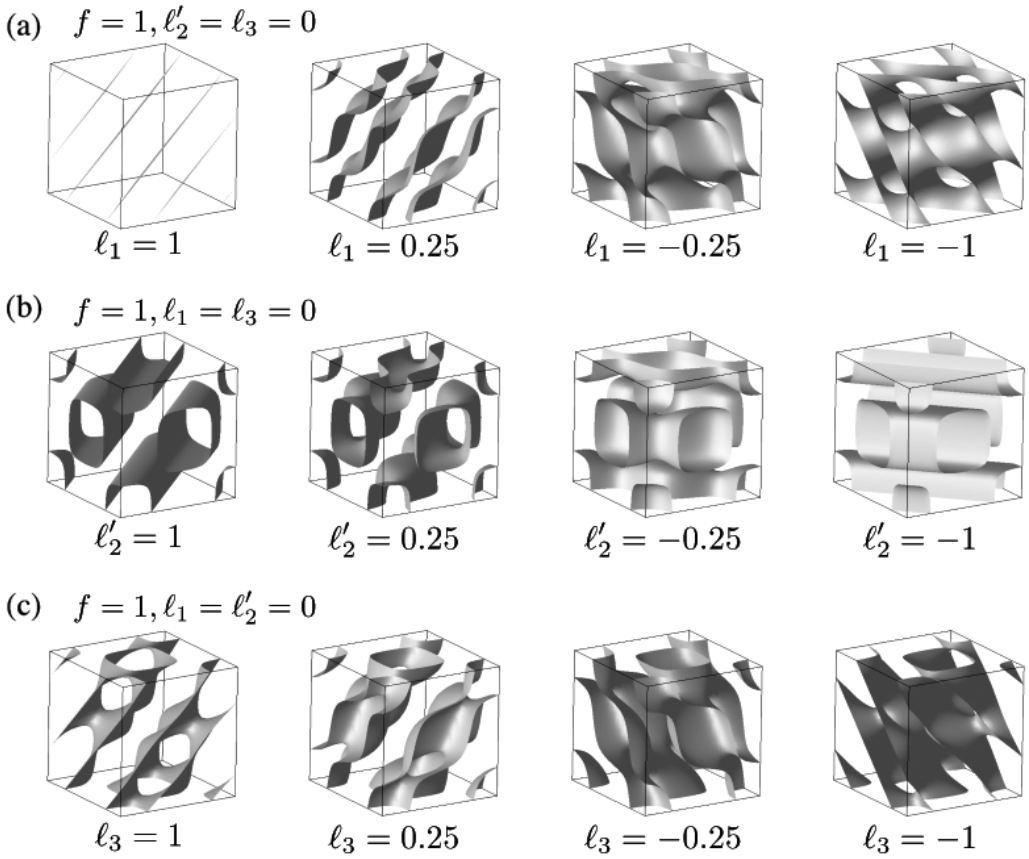

Figure 6. Structure obtained by adding the deviations in figure 5 to the fcc structure of the one-mode expression in the isosurface representation with $\phi_{\mathrm{ISO}} = 1.0$ by changing the values of (a) ℓ_1, (b) ℓ_2', and (c) ℓ_3. If the magnitudes of the deviation are equivalent to that of the fcc structure, the structures become lamellar ((a) $\ell_1 = 1$), diamond ((a) $\ell_1 = -1$), distorted cylinder ((b) $\ell_2' = \pm 1$), and perforated lamellar ((c) $\ell_3 = \pm 1$) structures.

gives the solution $b_i = -5.335\,30 \times 10^{-2}$ $(i = 1, \ldots, 6)$ and $b_j = -2.452\,35 \times 10^{-3}$ $(j = 7, 8, 9)$.

The essential difference of the mode expansion for bcc and fcc can be seen in the reduced amplitude equations. Substituting $b_i = C$ $(i = 1, \ldots, 6)$ and $b_j = D (j = 7, 8, 9)$ into equations (A.4) and (A.10), the following equations are obtained:

$$\frac{\mathrm{d}C}{\mathrm{d}t} = -P^2 g\big(\Gamma(P)C + 45C^3 + 36C^2 D + 24CD^2 + 12C^2\bar{\phi} + 12CD\bar{\phi}\big) \tag{26}$$

$$\frac{\mathrm{d}D}{\mathrm{d}t} = -2P^2 g\big(\Gamma(\sqrt{2}P)D + 24C^3 + 48C^2 D + 15D^3 + 12C^2\bar{\phi}\big). \tag{27}$$

The difference between equations (19) and (27) is the C^3 term in equation (27), which arises from the last term of equation (A.3). Because of this term, the amplitude D becomes zero for $\tau = 2\sqrt{\alpha} + 8.25\bar{\phi}^2 g$ with $C = -0.5\bar{\phi}$. This observation supports the fact that the magnitude of the peaks corresponding to the higher modes for the bcc structure are much smaller than those for the fcc structure in the weak segregation regime in figure 1.

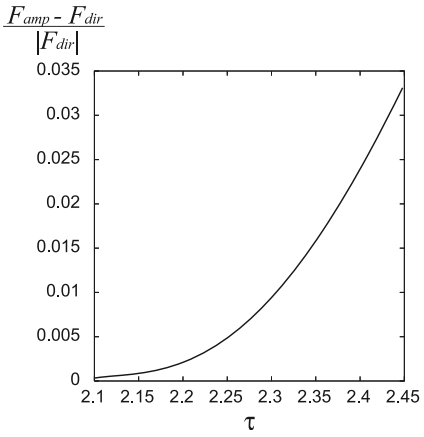

Figure 7. Plot of the free energy difference $(F_{\rm amp} - F_{\rm dir})/|F_{\rm dir}|$ versus τ, where $F_{\rm amp}$ and $F_{\rm dir}$ are obtained by equation (16) and equation (1), respectively.

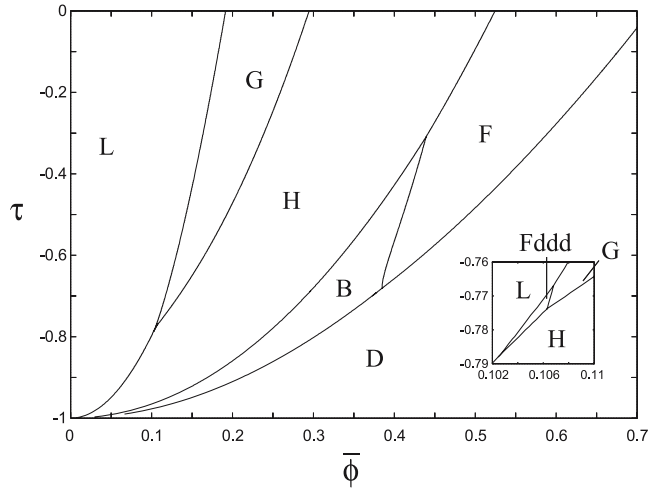

Figure 8. Phase diagram obtained by the direct simulation of equation (30). The regions indicated by L, G, H, B, F, and D are the stable phase of lamellae, gyroid, hexagons, bcc, fcc, and disorder, respectively. The inset is the enlargement near the triple point G, L, and H, where the $Fddd$ structure is the most stable.

Figure 7 shows the free energy difference $(F_{\rm amp} - F_{\rm dir})/|F_{\rm dir}|$ as a function of τ, where the free energy $F_{\rm amp}$ is obtained by substituting the equilibrium solutions of equations (8)–(14) into equation (16). In the same way, the free energy $F_{\rm dir}$ is obtained by introducing the solutions equation (4) into equation (1). It is obvious from this figure that the results in this section are valid only for a weak segregation regime. The accuracy of the mode expansion (6) decreases with increasing value of τ.

4. Summary and discussion

The stability of the fcc structure has been investigated by the simple free energy functional (1) for microphase separation. In the phase diagram obtained numerically, there is a region where the fcc structure is the most stable equilibrium structure. In the present simulations, the relaxation dynamics was applied to the size of the simulation box, which is valid for searching the equilibrium structures. The phase diagram was not altered qualitatively by changing the number of meshes as $64 \times 64 \times 64$. Furthermore, the amplitude equations were derived by the mode expansion method, which is valid in the weak segregation regime. The higher harmonic modes of the fcc symmetry were taken into account, and it was confirmed that the fcc structure could be formed at least as a metastable state. These results suggest that the formation of the fcc structure is possible experimentally if the system size is adjusted to the equilibrium period of the fcc structure.

The stability of the fcc structure has a distinct property compared to other structures that can be stable with the minimal number of modes to express the target structure. That is, one-mode expansions (two-mode expansions) are sufficient for expressing and stabilizing the bcc, hexagonal cylinder, and lamellar structures (gyroid and $Fddd$ structures) [7–10]. On the other hand, the fcc structure which is unstable without the higher modes becomes stable by taking account of the higher modes.

It is found by the mode expansion method that the fcc structure can be a metastable structure in a certain region in the weak segregation regime. However, these results are valid only for a weak segregation as shown in figure 7, because it is necessary to truncate the mode expansion up to a finite number. Therefore, direct numerical simulations of equation (4) are needed to investigate the stability propertied in a wider range of segregation, which is time consuming, but more reliable compared with the mode expansion truncated up to finite number of modes. In fact, the free energy of bcc evaluated by substituting the equilibrium solutions of equations (A.4)–(A.12) into equation (A.3) is smaller than that of fcc evaluated by substituting the equilibrium solutions of equations (8)–(14) into equation (16) even in the region where fcc is the most stable in figure 2.

We have verified that the present results are not specific for the free energy (1). For instance, if we employ the Brazovskii free energy [22]:

$$F[\phi] = \int {\rm d}\boldsymbol{r}\left[\frac{1}{2}(\nabla^2\phi)^2 - \frac{\beta}{2}(\nabla\phi)^2 - \frac{\tau}{2}\phi^2 + \frac{g}{4}\phi^4\right], \quad (28)$$

the function $\Gamma(x)$ in the mode expansion equations (8)–(14) is given by

$$\Gamma(x) = \frac{1}{g}\left(x^4 - \beta x^2 - \tau + 3\bar{\phi}^2 g\right). \quad (29)$$

This model free energy is used not only for phase separation in polymer [23, 24] but also for crystal [25], the nematic-to-smectic-C transition in liquid crystals [26], and Rayleigh–Bénard convection [27].

The time evolution equation with the free energy functional (28) is given by

$$\frac{\partial\phi}{\partial t} = \nabla^2(\nabla^4\phi + \beta\nabla^2\phi - \tau\phi + g\phi^3). \quad (30)$$

Figure 8 is the phase diagram obtained by performing the direct simulations of this evolution equation with $\beta = 2$ and $g = 1$. There is a wider region than that shown in figure 2, where the fcc structure is the most stable.

Acknowledgments

The author would like to thank T Ohta, S Majaniemi, T Uneyama, and K Yamada for valuable discussions. This study was supported by a Grant-in-Aid from the Ministry of Education, Science, and Culture of Japan.

Appendix

In the case of the bcc structure, the local volume fraction ϕ can be represented as

$$\phi(\boldsymbol{r}) = \bar{\phi} + 2\sum_{i=1}^{9} b_i \cos(\boldsymbol{p}_i \cdot \boldsymbol{r}) \tag{A.1}$$

where

$$\begin{aligned} \boldsymbol{p}_1 &= \frac{P}{\sqrt{2}}(0,1,1), & \boldsymbol{p}_2 &= \frac{P}{\sqrt{2}}(1,0,1), \\ \boldsymbol{p}_3 &= \frac{P}{\sqrt{2}}(1,1,0), & \boldsymbol{p}_4 &= \frac{P}{\sqrt{2}}(0,1,-1), \\ \boldsymbol{p}_5 &= \frac{P}{\sqrt{2}}(-1,0,1), & \boldsymbol{p}_6 &= \frac{P}{\sqrt{2}}(1,-1,0), \\ \boldsymbol{p}_7 &= \frac{P}{\sqrt{2}}(2,0,0), & \boldsymbol{p}_8 &= \frac{P}{\sqrt{2}}(0,2,0), \\ & & \boldsymbol{p}_9 &= \frac{P}{\sqrt{2}}(0,0,2). \end{aligned} \tag{A.2}$$

It is obvious that $|\boldsymbol{p}_i| = P$ $(i = 1, \ldots, 6)$ and $|\boldsymbol{p}_j| = \sqrt{2}P$ $(j = 7, 8, 9)$. The free energy for the bcc structure is given by

$$\begin{aligned} F_{\mathrm{bcc}} = F_{\mathrm{dis}} + g\Bigg[& \sum_{i=1}^{9} \Gamma(|\boldsymbol{p}_i|) b_i^2 + \frac{3}{2}\sum_{i=1}^{9} b_i^4 + 6\sum_{i=1}^{9}\sum_{j=i+1}^{9} b_i^2 b_j^2 \\ & + 12\bar{\phi} b_1 b_2 b_6 + 12\bar{\phi} b_1 b_3 b_5 + 12\bar{\phi} b_2 b_3 b_4 + 12\bar{\phi} b_4 b_5 b_6 \\ & + 12\bar{\phi} b_1 b_4 (b_8 + b_9) + 12\bar{\phi} b_2 b_5 (b_7 + b_9) \\ & + 12\bar{\phi} b_3 b_6 (b_7 + b_8) + 12 b_1 b_2 b_4 b_5 + 12 b_1 b_3 b_4 b_6 \\ & + 12 b_2 b_3 b_5 b_6 + 6(b_6^2 + b_3^2) b_7 b_8 + 6(b_4^2 + b_1^2) b_8 b_9 \\ & + 6(b_5^2 + b_2^2) b_7 b_9 + 12(b_1 b_2 b_3 + b_2 b_4 b_6 \\ & + b_3 b_4 b_5 + b_1 b_5 b_6)(b_7 + b_8 + b_9) \Bigg]. \end{aligned} \tag{A.3}$$

The equations for amplitude are given by

$$\begin{aligned} \frac{\mathrm{d}b_1}{\mathrm{d}t} = -|\boldsymbol{p}_1|^2 g \Bigg[& \Gamma(|\boldsymbol{p}_1|) b_1 - 3b_1^3 \\ & + 6b_1 \sum_{i=1}^{9} b_i^2 + 6\bar{\phi} b_2 b_6 + 6\bar{\phi} b_3 b_5 + 6\bar{\phi} b_4 b_8 + 6\bar{\phi} b_4 b_9 \\ & + 6 b_1 b_8 b_9 + 6 b_2 b_3 b_7 + 6 b_2 b_3 b_8 + 6 b_2 b_3 b_9 + 6 b_2 b_4 b_5 \\ & + 6 b_3 b_4 b_6 + 6 b_5 b_6 b_7 + 6 b_5 b_6 b_8 + 6 b_5 b_6 b_9 \Bigg] \end{aligned} \tag{A.4}$$

$$\begin{aligned} \frac{\mathrm{d}b_2}{\mathrm{d}t} = -|\boldsymbol{p}_2|^2 g \Bigg[& \Gamma(|\boldsymbol{p}_2|) b_2 - 3b_2^3 \\ & + 6b_2 \sum_{i=1}^{9} b_i^2 + 6\bar{\phi} b_1 b_6 + 6\bar{\phi} b_3 b_4 + 6\bar{\phi} b_5 b_7 + 6\bar{\phi} b_5 b_9 \\ & + 6 b_1 b_3 b_7 + 6 b_1 b_3 b_8 + 6 b_1 b_3 b_9 + 6 b_1 b_4 b_5 + 6 b_2 b_7 b_9 \\ & + 6 b_3 b_5 b_6 + 6 b_4 b_6 b_7 + 6 b_4 b_6 b_8 + 6 b_4 b_6 b_9 \Bigg] \end{aligned} \tag{A.5}$$

$$\begin{aligned} \frac{\mathrm{d}b_3}{\mathrm{d}t} = -|\boldsymbol{p}_3|^2 g \Bigg[& \Gamma(|\boldsymbol{p}_3|) b_3 - 3b_3^3 \\ & + 6b_3 \sum_{i=1}^{9} b_i^2 + 6\bar{\phi} b_1 b_5 + 6\bar{\phi} b_2 b_4 + 6\bar{\phi} b_6 b_7 + 6\bar{\phi} b_6 b_8 \\ & + 6 b_1 b_2 b_7 + 6 b_1 b_2 b_8 + 6 b_1 b_2 b_9 + 6 b_1 b_4 b_6 + 6 b_2 b_5 b_6 \\ & + 6 b_3 b_7 b_8 + 6 b_4 b_5 b_7 + 6 b_4 b_5 b_8 + 6 b_4 b_5 b_9 \Bigg] \end{aligned} \tag{A.6}$$

$$\begin{aligned} \frac{\mathrm{d}b_4}{\mathrm{d}t} = -|\boldsymbol{p}_4|^2 g \Bigg[& \Gamma(|\boldsymbol{p}_4|) b_4 - 3b_4^3 \\ & + 6b_4 \sum_{i=1}^{9} b_i^2 + 6\bar{\phi} b_1 b_8 + 6\bar{\phi} b_1 b_9 + 6\bar{\phi} b_2 b_3 + 6\bar{\phi} b_5 b_6 \\ & + 6 b_1 b_2 b_5 + 6 b_1 b_3 b_6 + 6 b_2 b_6 b_7 + 6 b_2 b_6 b_8 + 6 b_2 b_6 b_9 \\ & + 6 b_3 b_5 b_7 + 6 b_3 b_5 b_8 + 6 b_3 b_5 b_9 + 6 b_4 b_8 b_9 \Bigg] \end{aligned} \tag{A.7}$$

$$\begin{aligned} \frac{\mathrm{d}b_5}{\mathrm{d}t} = -|\boldsymbol{p}_5|^2 g \Bigg[& \Gamma(|\boldsymbol{p}_5|) b_5 - 3b_5^3 \\ & + 6b_5 \sum_{i=1}^{9} b_i^2 + 6\bar{\phi} b_1 b_3 + 6\bar{\phi} b_2 b_7 + 6\bar{\phi} b_2 b_9 + 6\bar{\phi} b_4 b_6 \\ & + 6 b_1 b_2 b_4 + 6 b_1 b_6 b_7 + 6 b_1 b_6 b_8 + 6 b_1 b_6 b_9 + 6 b_2 b_3 b_6 \\ & + 6 b_3 b_4 b_7 + 6 b_3 b_4 b_8 + 6 b_3 b_4 b_9 + 6 b_5 b_7 b_9 \Bigg] \end{aligned} \tag{A.8}$$

$$\begin{aligned} \frac{\mathrm{d}b_6}{\mathrm{d}t} = -|\boldsymbol{p}_6|^2 g \Bigg[& \Gamma(|\boldsymbol{p}_6|) b_6 - 3b_6^3 \\ & + 6b_6 \sum_{i=1}^{9} b_i^2 + 6\bar{\phi} b_1 b_2 + 6\bar{\phi} b_3 b_7 + 6\bar{\phi} b_3 b_8 + 6\bar{\phi} b_4 b_5 \\ & + 6 b_1 b_3 b_4 + 6 b_1 b_5 b_7 + 6 b_1 b_5 b_8 + 6 b_1 b_5 b_9 + 6 b_2 b_3 b_5 \\ & + 6 b_2 b_4 b_7 + 6 b_2 b_4 b_8 + 6 b_2 b_4 b_9 + 6 b_6 b_7 b_8 \Bigg] \end{aligned} \tag{A.9}$$

$$\begin{aligned} \frac{\mathrm{d}b_7}{\mathrm{d}t} = -|\boldsymbol{p}_7|^2 g \Bigg[& \Gamma(|\boldsymbol{p}_7|) b_7 - 3b_7^3 \\ & + 6b_7 \sum_{i=1}^{9} b_i^2 + 6\bar{\phi} b_2 b_5 + 6\bar{\phi} b_3 b_6 \\ & + 3b_2^2 b_9 + 3b_3^2 b_8 + 3b_5^2 b_9 + 3b_6^2 b_8 \\ & + 6 b_1 b_2 b_3 + 6 b_1 b_5 b_6 + 6 b_2 b_4 b_6 + 6 b_3 b_4 b_5 \Bigg] \end{aligned} \tag{A.10}$$

$$\begin{aligned} \frac{\mathrm{d}b_8}{\mathrm{d}t} = -|\boldsymbol{p}_8|^2 g \Bigg[& \Gamma(|\boldsymbol{p}_8|) b_8 - 3b_8^3 \\ & + 6b_8 \sum_{i=1}^{9} b_i^2 + 6\bar{\phi} b_1 b_4 + 6\bar{\phi} b_3 b_6 \\ & + 3b_1^2 b_9 + 3b_3^2 b_7 + 3b_4^2 b_9 + 3b_6^2 b_7 \\ & + 6 b_1 b_2 b_3 + 6 b_1 b_5 b_6 + 6 b_2 b_4 b_6 + 6 b_3 b_4 b_5 \Bigg] \end{aligned} \tag{A.11}$$

$$\frac{\mathrm{d}b_9}{\mathrm{d}t} = -|\boldsymbol{p}_9|^2 g\Bigg[\Gamma(|\boldsymbol{p}_9|)b_9 - 3b_9^3 + 6b_9\sum_{i=1}^{9} b_i^2 + 6\bar{\phi}b_1b_4 + 6\bar{\phi}b_2b_5 + 3b_1^2b_8 + 3b_2^2b_7 + 3b_4^2b_8 + 3b_5^2b_7 + 6b_1b_2b_3 + 6b_1b_5b_6 + 6b_2b_4b_6 + 6b_3b_4b_5\Bigg], \qquad \text{(A.12)}$$

where the function $\Gamma(x)$ is given by equation (15).

References

[1] Bang J, Lodge T P, Wang X, Brinker K L and Burghardt W R 2002 *Phys. Rev. Lett.* **89** 215505
[2] Lodge T P, Pudil B and Hanley K J 2002 *Macromolecules* **35** 4707–17
[3] Huang Y-Y, Hsu J-Y, Chen H-L and Hashimoto T 2007 *Macromolecules* **40** 3700–7
[4] Imaizumi K, Ono T, Kota T, Okamoto S and Sakurai S 2003 *J. Appl. Crystallogr.* **36** 976–81
[5] Qi S and Wang Z-G 1996 *Phys. Rev. Lett.* **76** 1679–82
[6] Qi S and Wang Z-G 1997 *Phys. Rev.* E **55** 1682–97
[7] Nonomura M and Ohta T 2001 *J. Phys.: Condens. Matter* **13** 9089–112
[8] Yamada K, Nonomura M and Ohta T 2004 *Macromolecules* **37** 5762–77
[9] Yamada K, Nonomura M, Saeki A and Ohta T 2005 *J. Phys.: Condens. Matter* **17** 4877–87
[10] Yamada K, Nonomura M and Ohta T 2006 *J. Phys.: Condens. Matter* **18** L421–7
[11] Tyler C A and Morse D C 2005 *Phys. Rev. Lett.* **94** 208302
[12] Fredrickson G H 2006 *The Equilibrium Theory of Inhomogeneous Polymers* (Oxford University Press)
[13] Matsen M W and Bates F S 1996 *Macromolecules* **29** 1091–8
[14] Matsen M W and Bates F S 1996 *Macromolecules* **29** 7641–4
[15] Ohta T and Kawasaki K 1986 *Macromolecules* **19** 2621–32
[16] Bahiana M and Oono Y 1990 *Phys. Rev.* A **41** 6763–71
[17] Choksi R and Ren R 2003 *J. Stat. Phys.* **113** 151–74
[18] Eyre D J 1998 http://www.math.utah.edu/∼eyre/research/methods/stable.ps
[19] Honda T and Kawakatsu T 2006 *Macromolecules* **39** 2340–9
[20] Cullity B D and Stock S R 2001 *Elements of X-ray Diffraction* (Englewood Cliffs, NJ: Prentice-Hall) chapter 10
[21] Chaikin P M and Lubensky T C 1995 *Principles of Condensed Matter Physics* (Cambridge University Press) chapter 4
[22] Brazovskii S A 1975 *Sov. Phys.—JETP* **41** 85
[23] Leibler L 1980 *Macromolecules* **13** 1602–17
[24] Hamley I W and Podneks V E 1997 *Macromolecules* **30** 3701–3
[25] Elder K R, Katakowski M, Haataja M and Grant M 2002 *Phys. Rev. Lett.* **88** 245701
[26] Swift J 1976 *Phys. Rev.* A **14** 2274–7
[27] Swift J and Hohenberg P C 1977 *Phys. Rev.* A **15** 319–28